

# Thermic effects on the resonance fluorescence of doubly dressed artificial atoms

David F. Macias-Pinilla and Hanz Y. Ramírez\*

*Grupo de Física Teórica y Computacional, Escuela de Física,  
Universidad Pedagógica y Tecnológica de Colombia (UPTC), Tunja 150003, Boyacá, Colombia.*  
(Dated: October 10, 2016)

In this work, operation robustness of controlled density of optical states under phonon dissipation is studied for an artificial atom simultaneously driven by two distinguishable fields. We investigate the influence of carrier-phonon interaction on the emission properties of the doubly driven two-level system by using both, perturbative and polaron approaches. Phonon effects are evidenced through comparing emission spectra obtained for finite temperatures, with that calculated at zero temperatures where lattice vibrations are absent.

## INTRODUCTION

Semiconductors quantum dots (QDs) or “artificial atoms”, have completely quantized energy states which allows selective probing of particular exciton (electron-hole pair) transitions. The properties of QDs are a topical trend given its importance for essential scientific research and technological applications [1]. Between different types of QDs currently under investigation, this study focuses on self-assembled *InAs/GaAs* QDs [2]. These materials have similar lattice parameters and a difference in energy gaps that guarantees the existence of bound states. Phonon interactions in QDs constitute a limitation on the level of coherence in their excitonic transitions. The phonon-induced dephasing process is responsible for the intensity damping of QDs exciton Rabi rotations [3].

Two-level quantum system irradiated by a monochromatic field under resonant excitation, presents a distinct stimulated emission [resonance fluorescence (RF)], so called Mollow triplet [4]. Emission properties in the case of QDs were studied considering a single QD as a two-level system with unexcited crystal ground state and single-exciton state [5, 6]. That system was exposed to strong driving fields, clearly showing the same RF spectrum of an atom. The radiative properties of two-level quantum system driven by monochromatic fields (one strong and one weaker) were described using the doubly dressed atom model, first coupling the bare atom to the stronger field, and then coupling the dressed states to the weaker field. RF spectrum (RFS) was found by the real part of the Fourier transform of the two-time correlation function of the dipole-moment operator [7]. In mid-2015, RF spectrum for two-level system driven by monochromatic fields was demonstrated experimentally for QDs in full agreement with the predictions for real and artificial atoms [8, 9].

The experimental RF in QDs presents a systematic spectral sideband broadening due to the interactions of the dressed excitons with the phonon reservoir, that can be observed with increasing temperature [10]. Precisely are these dissipation effects on the RF of a QD driven

by two distinguishable fields what we study here, based on the influence of phonons on the incoherent emission spectrum, that can be captured entirely by damping of the QD excitonic Rabi frequency and the introduction of a pure-dephasing rate [11].

This work is structured as follows. In the first section, RF of a doubly driven QDs, is introduced. In the following sections, the phonon effects on the RF of a QD driven by two distinguishable fields are presented, and results are formulated.

## DOUBLY DRESSED STATES

We consider a two level excited system by two distinguishable lasers, one strong and the other one much weaker. The fields have the same frequency  $\omega_L$ , and Rabi frequencies  $2\Omega$  (strong field) and  $2G$  (weak field). Theoretically, the atom is first coupled to the strong field, then the dressed system is coupled to the weak field, and finally the doubly dressed system decays spontaneously into the vacuum field [12]. This model is valid in the limits  $\omega_L \approx \omega_0 \gg 2\Omega > 2G > \Gamma$ .

In resonance, the Hamiltonian  $\hat{H}_d = \hat{H}_{AF} + \hat{H}_W$  that includes interaction with the stronger laser but not with the weak one, has eigenstates  $|i, N - n, n\rangle$  ( $i = 1, 2$ ), that satisfy the eigenvalue equation [13]

$$\hat{H}_d|i, N - n, n\rangle = \hbar[N\omega_L - (-1)^i\Omega]|i, N - n, n\rangle, \quad (1)$$

where the numbers  $N$  and  $n$ , are the total number of photons and number of photons associated to the weak field, respectively. The interaction between the dressed system and the weaker field is included as

$$\hat{V}_C = \hbar g_1(\hat{a}^\dagger \hat{S}_- + \hat{a} \hat{S}_+). \quad (2)$$

For  $\Gamma > G$ , the coupling with the weak field generates a set of states along an energy range of  $2G$  (see figure 1). The interaction  $\hat{V}_C$  has the following matrix elements

$$\begin{aligned} V_{nm}^{(i)} &= \langle i, N - n; n | \hat{V}_C | i, N - m; m \rangle, \\ &= -(-1)^i \hbar g_n (\sqrt{n+1} \delta_{n+1,m} + \sqrt{n} \delta_{n-1,m}), \end{aligned} \quad (3)$$

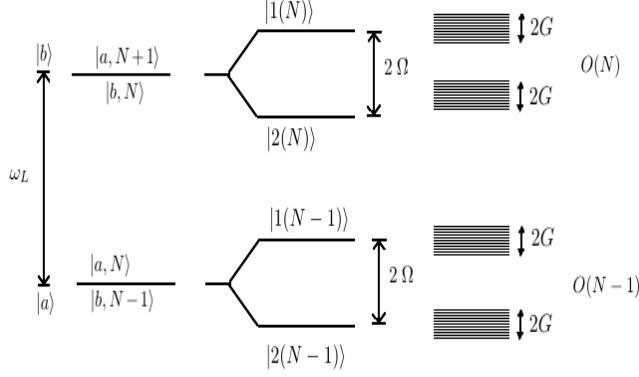


FIG. 1. Doubly dressed states.

where  $g_n = g_1 \sin \theta \cos \theta$ . This matrix has the same form of the position operator in the basis of energy eigenstates of the one-dimensional harmonic oscillator [14], and its eigenvalues are written as  $-(-1)^i \lambda \hbar g_n$ ,  $-\infty < \lambda < \infty$ . With these assumptions, the total Hamiltonian of the system satisfies the eigenvalue equation

$$(\hat{H}_d + \hat{V})|Ni\lambda\rangle = E_{N\lambda}^{(i)}|Ni\lambda\rangle, \quad (4)$$

where

$$E_{N\lambda}^{(i)} = \hbar[N\omega_L - (-1)^i(\Omega + \lambda g_n)], \quad (5)$$

$$|Ni\lambda\rangle = \sum_{n=0}^{\infty} \phi_n[-(-1)^i \frac{\lambda}{\sqrt{2}}]|i, N-n; n\rangle, \quad (6)$$

and

$$\phi_n(x) = (\sqrt{2\pi}2^n n!)^{-1/2} H_n(x) e^{(-\frac{1}{2}x^2)}, \quad (7)$$

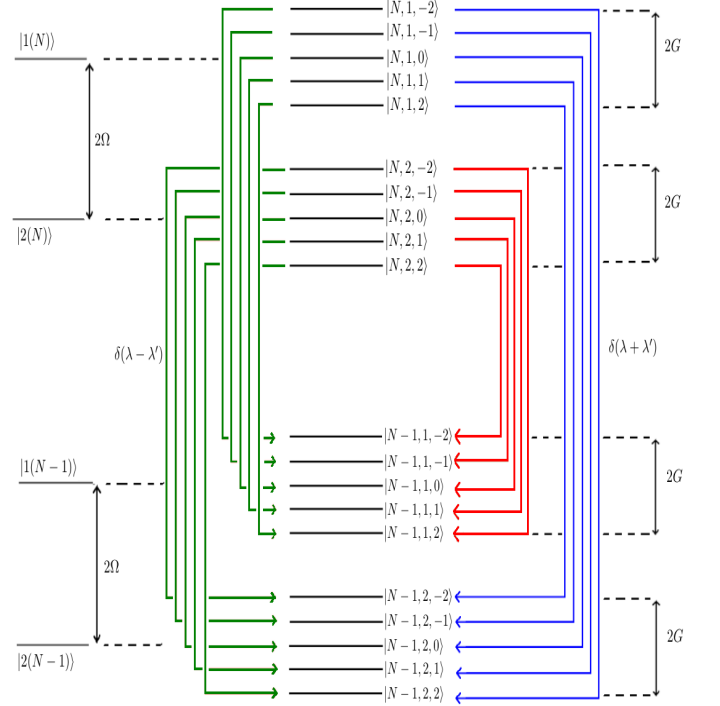
which is the harmonic oscillator eigenfunction  $\phi_n(x)$ , containing the Hermite polynomial  $H_n(x)$  of order  $n$ . The eigenvectors in equation (6) satisfy the orthonormality and completeness relations, and they are used to find the nonvanishing matrix elements of the atomic transition operator  $\hat{S}_+$ , as

$$\langle N1\lambda|\hat{S}_+|(N-1)2\lambda'\rangle = (1/2)\delta(\lambda + \lambda'), \quad (8)$$

$$\langle N2\lambda|\hat{S}_+|(N-1)1\lambda'\rangle = -(1/2)\delta(\lambda + \lambda'), \quad (9)$$

$$\langle Ni\lambda|\hat{S}_+|(N-1)i\lambda'\rangle = -(-1)^i(1/2)\delta(\lambda - \lambda'). \quad (10)$$

Sign differences in the delta functions correspond to different features between the central and the side components of the RFS. From equations (8) and (9), we can see that the allowed transitions are those that satisfying  $\lambda = -\lambda'$ . Because of this, transitions with various energies are generated and the sidebands in the RFS present broadening (see figure 2). In contrast, from equation

FIG. 2. Spontaneous transitions between doubly dressed states, with a finite set of states ( $-2 < \lambda < 2$ ).

(10), transitions are governed by  $\lambda = \lambda'$ , and these transitions have a unique energy, whereby the central peak is unmodified. The RFS is obtained from the real part of the Fourier transform of the two-time correlation function of the dipole-moment operator and is given by [7]

$$L_d(\omega) = \frac{\Gamma}{4\pi} \left\{ \frac{\Gamma/2}{(\omega - \omega_L)^2 + (\Gamma/2)^2} + \frac{1}{4} \int_{-\infty}^{+\infty} d\lambda |\phi_M(\lambda/\sqrt{2})|^2 \left( \frac{3\Gamma/4}{(\omega - \omega_L - 2\Omega - 2\lambda g_n)^2 + (3\Gamma/4)^2} + \frac{(3\Gamma/4)}{(\omega - \omega_L + 2\Omega - 2\lambda g_n)^2 + (3\Gamma/4)^2} \right) \right\}, \quad (11)$$

Coupling is given by  $g_n = \frac{\sin \theta \cos \theta G}{\sqrt{M}}$ , with  $M$  the number of photons in the weak field. The RFS in equation (11) is plotted in figure 3 and clearly shows how the sidebands present broadening (to an extent of  $2G$ ), while the central peak is unmodified.

RFS for a QD driven simultaneously by two electromagnetic fields, has been experimentally studied on an *InAs/GaAs* QD on states  $|0\rangle$  and  $|X\rangle$ . The QD was simultaneously excited to Rabi frequencies  $2\Omega = 2\pi \times 5$  GHz and  $2G = 2\pi \times 2$  GHz, respectively. The power ratio is given by  $\alpha = \frac{G}{\Omega} = 0.4$  (the power of the stronger laser was 100  $\mu W$ ). The QD is embedded in a low-Q planar microcavity ( $Q \approx 200$ ) and a cryostat bath at 4.2 K (see figure 4 (a)). The result of the experiment

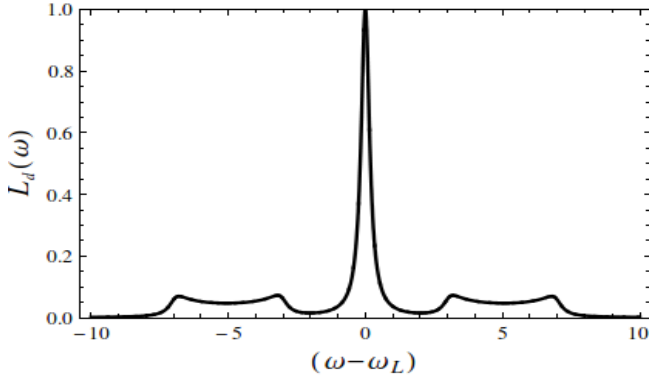


FIG. 3. Normalized RFS for a two-level system driven by two fields. The Hermite polynomial of order  $M = 40$  is used,  $\delta_L = 0$ ,  $2\Omega = 2\pi \times 5$  GHz,  $2G = 2\pi \times 2$  GHz and  $\Gamma = 2.35$  GHz.

is a RFS consistent with that of in equation (11) [9] (the experiment does not consider dephasing due to phonons).

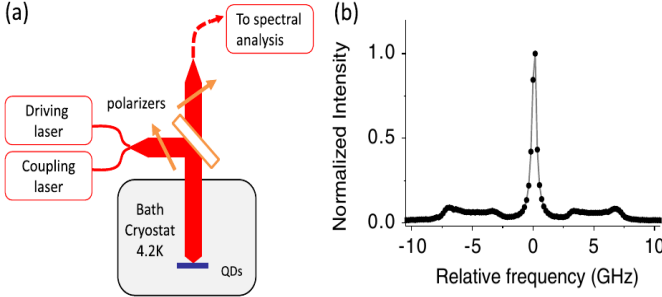


FIG. 4. (a) Experimental set up. (b) Measured RFS of a QD driven by two electromagnetic fields, with  $2\Omega = 2\pi \times 5$  GHz,  $2G = 2\pi \times 2$  GHz and  $\Gamma \approx 2.35$  GHz

### TEMPERATURE-DEPENDENT RFS FROM A DOUBLY DRIVEN QD

We consider a two-level QD with ground state  $|0\rangle$  and exciton state  $|X\rangle$ , and an energy gap  $\hbar\omega_0$ . The QD is driven by a laser of frequency  $\omega_l \approx \omega_0$ , and Rabi frequency  $\Omega$ . The QD is coupled to a phonon bath represented by an infinite collection of harmonic oscillators of frequency  $\omega_k$ , and creation and annihilation operators,  $\hat{b}_k^\dagger$  and  $\hat{b}_k$ , respectively. Because the electron moves into the QD (crystal), this generates a deformation in the crystal lattice resulting in a polaronic system. In the continuum limit the system-bath interaction is characterized by the spectral density function [15]

$$J(\omega) = \alpha\omega^3 e^{(\omega/\omega_c)^2}, \quad (12)$$

that describes coupling to longitudinal acoustic (LA) phonons via deformation potential [16]. The coupling

constant  $\alpha$ , is the strength of the exciton-phonon interaction and depends on the characteristics of the QD. The phonon cutoff frequency is given by  $\omega_c$  and arises from the form factor of carrier wavefunctions.

The master equation that describes the dynamics of the system is developed in the Markov approximation and under the polaron transform [17–19]. This is given by

$$\begin{aligned} \frac{d\hat{\rho}(t)}{dt} = & -\frac{i}{2}[\Omega_r\hat{\sigma}_x, \hat{\rho}(t)] - \frac{\Omega^2}{4} \int_0^\infty d\tau \left( [\hat{\sigma}_x, \hat{\sigma}_x\hat{\rho}(t)]\Lambda_x(\tau) \right. \\ & + \cos(\Omega_r\tau)[\hat{\sigma}_y, \hat{\sigma}_y\hat{\rho}(t)]\Lambda_y(\tau) \\ & \left. + \sin(\Omega_r\tau)[\hat{\sigma}_y, \hat{\sigma}_z\hat{\rho}(t)]\Lambda_y(\tau) + \hat{H}.c. \right), \quad (13) \end{aligned}$$

where resonant excitation  $\delta' = 0$  has been considered,  $\hat{\sigma}_x = (|X\rangle\langle 0| + |0\rangle\langle X|)$ ,  $\hat{\sigma}_y = i(|0\rangle\langle X| - |X\rangle\langle 0|)$ , and  $\hat{\sigma}_z = (|X\rangle\langle X| + |0\rangle\langle 0|)$ , are the Pauli matrices. The term  $\Omega_r$  is included, which term corresponds to the renormalized Rabi frequency  $\Omega_r = \Omega B$ .

The stationarity of the reference state of the phonon bath in the continuum limit, are expressed as

$$\Lambda_x(\tau) = \frac{B^2}{2}(e^{\phi(\tau)} + e^{-\phi(\tau)} - 2), \quad (14)$$

$$\Lambda_y(\tau) = \frac{B^2}{2}(e^{\phi(\tau)} - e^{-\phi(\tau)}), \quad (15)$$

where the phonon correlation function  $\phi(\tau)$  is defined as [20]

$$\phi(\tau) = \int_0^\infty d\omega \frac{J(\omega)}{\omega} (\cos(\omega\tau) \coth(\beta\omega/2) - i \sin(\omega\tau)). \quad (16)$$

and the thermally averaged phonon displacement operator, is written as (LA)

$$\langle \hat{B}_\pm \rangle \equiv B = \exp \left[ -\frac{1}{2} \int_0^\infty d\omega \frac{J(\omega)}{\omega^2} \coth(\beta\omega/2) \right], \quad (17)$$

where  $\beta = 1/(k_B T)$ . In turn, the polaron frequency shift in the continuum limit is given by  $\Delta_p = \int_0^\infty d\omega J(\omega)/\omega$ .

### Damping rates

The damping rates in the polaron theory and the weak coupling approach, are obtained by the master equation 13. This damping rates are taking from the evolution of the Bloch vector in the polaron framework [19]. The base rates in this approach are

$$\Gamma_y = \frac{\Omega^2}{2} \gamma_x(0), \quad (18)$$

and

$$\Gamma_z = \frac{\Omega^2}{4}(\gamma_y(\Omega_r) + \gamma_y(-\Omega_r) + 2\gamma_x(0)), \quad (19)$$

where

$$\gamma_l(\omega) = 2\text{Re}[K_l(\omega)], \quad (20)$$

and the polaron response function is

$$K_l(\omega) = \int_0^\infty d\tau e^{i\omega\tau} \Lambda_l(\tau). \quad (21)$$

#### Weak coupling rate

From the Born-Markov treatment [15], the damping rate is expressed in the form

$$\Gamma_W = \frac{1}{4}(\gamma_W(\Omega) + \gamma_W(-\Omega)). \quad (22)$$

With a weak-coupling correlation function of the form

$$\Lambda_W(\tau) = \int_0^\infty d\omega J(\omega)(\cos(\omega\tau) \coth(\beta\omega/2) - i\sin(\omega\tau)), \quad (23)$$

the weak-coupling rate takes the form

$$\Gamma_W = \frac{\pi}{2}J(\Omega) \coth(\beta\Omega/2). \quad (24)$$

The weak-coupling rate has a linear temperature dependence in the high-temperature regime (see figure ??). This rate depends on the original Rabi frequency  $\Omega$  and does not take into account its renormalization.

#### Full polaron and single-phonon polaron rate

In the full polaron theory, the damping rate is given by the sum of  $\Gamma_y$  and  $\Gamma_z$  [19], as

$$\Gamma_p = \Gamma_y + \Gamma_z. \quad (25)$$

Using equations (18) and (19), we have

$$\Gamma_p = \frac{\Omega^2}{2}\gamma_x(0) + \frac{\Omega^2}{4}(\gamma_y(\Omega_r) + \gamma_y(-\Omega_r) + 2\gamma_x(0)),$$

$$\Gamma_p = \frac{\Omega^2}{4}(\gamma_y(\Omega_r) + \gamma_y(-\Omega_r) + 4\gamma_x(0)),$$

and taking into account equations (20) and (21), then

$$\Gamma_p = \frac{\Omega^2}{4}(2\text{Re}[K_y(\Omega_r)] + 2\text{Re}[K_y(-\Omega_r)] + 4(2\text{Re}[K_x(0)])),$$

$$\Gamma_p = \frac{\Omega^2}{4} \left( 2\text{Re} \left[ \int_0^\infty d\tau e^{i\Omega_r\tau} \Lambda_y(\tau) \right] \right.$$

$$\left. + 2\text{Re} \left[ \int_0^\infty d\tau e^{-i\Omega_r\tau} \Lambda_y(\tau) \right] + 4 \left( 2\text{Re} \left[ \int_0^\infty d\tau \Lambda_x(\tau) \right] \right) \right).$$

Inserting the phonon correlation functions from equations (14) and (15), the full polaron rate is found as

$$\Gamma_p = \frac{\Omega_r^2}{4} \left( \text{Re} \left[ \int_0^\infty d\tau e^{i\Omega_r\tau} (e^{\phi(\tau)} - e^{-\phi(\tau)}) \right] \right. \\ \left. + \text{Re} \left[ \int_0^\infty d\tau e^{-i\Omega_r\tau} (e^{\phi(\tau)} - e^{-\phi(\tau)}) \right] \right. \\ \left. + 4\text{Re} \left[ \int_0^\infty d\tau (e^{\phi(\tau)} + e^{-\phi(\tau)} - 2) \right] \right). \quad (26)$$

Now to find the single-phonon polaron rate, we take the truncated expansion  $e^{\pm\phi(\tau)} = 1 \pm \phi(\tau)$ , obtaining

$$\Gamma_{1-ph} = \frac{\Omega_r^2}{4} \left( 2\text{Re} \left[ \int_0^\infty d\tau e^{i\Omega_r\tau} \phi(\tau) \right] \right. \\ \left. + 2\text{Re} \left[ \int_0^\infty d\tau e^{-i\Omega_r\tau} \phi(\tau) \right] \right),$$

this equation can be written in closed form as [10]

$$\Gamma_{1-ph} = \frac{\pi}{2}J(\Omega_r) \coth(\beta\Omega_r/2). \quad (27)$$

The single-phonon polaron rate has the same form as the weak-coupling rate, but differs in that the former one takes into account the renormalized Rabi frequency  $\Omega_r$ . The  $\Gamma_W$ ,  $\Gamma_{ph-1}$  and  $\Gamma_p$  rates have similar behavior at low temperatures ( $T < 10 - 15$  K), however at high temperatures split noticeably, and multiphonon effects described by the polaron rate, become important. In addition the  $\Gamma_{1-ph}$  rate decreases at high temperatures confirming that underestimates the coupling with phonons.

## RESULTS

Dissipation effects by phonons (DEBPs) on the incoherent emission spectrum are captured entirely by a renormalization of the original Rabi frequencies and the introduction of damping rates [10]. We use the spectrum in equation (11), the original and renormalized Rabi frequencies, and the  $\Gamma_W$ ,  $\Gamma_{ph-1}$  and  $\Gamma_p$  damping rates, to observe effects due to phonons. As previously discussed, equation (11) corresponds to a two level system driven by two fields modes, one strong and one weak, with Rabi frequencies  $\Omega$  and  $G$ , respectively. Because the Rabi frequency  $G$  is weaker than  $\Omega$ , its contribution to the damping rates is neglected and only its renormalization,  $G_r = GB$ , is considered (see figure 5).

We use parameters correspond to a single self-assembled InAs/GaAs QD embedded in a microcavity with a low  $Q$  factor ( $\sim 200$ ). The Rabi frequency  $2\Omega$

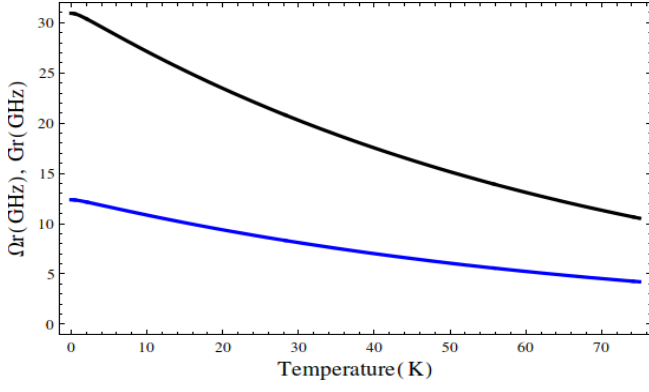


FIG. 5. Temperature dependence of renormalized Rabi frequencies  $\Omega_r$  (black line) and  $G_r$  (blue line).

is tuned to  $2\pi \times 5$  GHz and the Rabi frequency  $2G$  to  $2\pi \times 2$  GHz. The spontaneous emission rate of the neutral exciton state is given by  $\Gamma = 2.35$  GHz. The coupling constant is taken as  $\alpha = 2.535 \times 10^{-7}$  GHz $^{-2}$  and the phonon cutoff frequency as  $\omega_c \approx 493.33$  GHz [10].

#### DEBPs on the RFS of a QD driven by two fields in the weak-coupling rate

To calculate the RFS for a single QD driven by two electromagnetic fields in the exciton-phonon weak-coupling limit, the damping rate  $\Gamma_W$  is included in the spectrum (11), as

$$\Gamma_T = \Gamma + \frac{\pi}{2} J(\Omega) \coth(\Omega/2k_B T). \quad (28)$$

Carrying out the calculation for various temperatures,

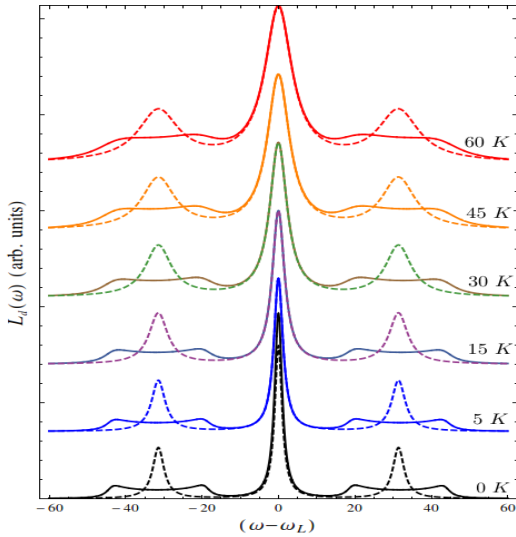


FIG. 6. DEBPs on the RFS of a QD driven by one (dashed lines) and two (solid lines) electromagnetic fields in the weak limit  $\Gamma_W$ .

the phonon effects can be elucidated. In figure 6, we see the DEBPs on the RFS of a monochromatically doubly driven QD (the case of single driving is added in dashed lines for comparison), for a temperature range between 0 and 60 K. The weak-coupling does not renormalize the Rabi frequencies, then the peak positions remains unchanged. Peaks are deformed and broadened, and their intensities decrease with the increasing temperature.

#### DEBPs on the RFS for a QD driven by two fields in the single-phonon polaron limit

In the single-phonon polaron limit, the Rabi frequencies ( $\Omega$  and  $G$ ) are renormalized as

$$\Omega_r = \Omega B \quad \text{and} \quad G_r = GB,$$

and the total damping rate is given by

$$\Gamma_T = \Gamma + \Gamma_{1-ph},$$

$$\Gamma_T = \Gamma + \frac{\pi}{2} J(\Omega_r) \coth(\Omega_r/2k_B T). \quad (29)$$

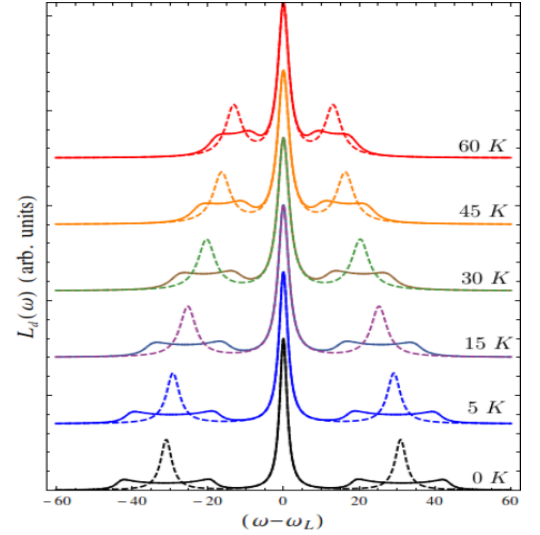


FIG. 7. DEBPs on the RFS of a QD driven by one (dashed lines) and two (solid lines) electromagnetic fields within the single-phonon polaron limit.

In this limit, DEBPs on the RFS of a doubly driven QD are mainly manifested by the stronger sideband deformation. The sidebands move towards the central peak and their width decreases with increasing temperature. At high temperatures ( $T > 40$  K) the damping rate decreases, and the peak intensity tends to stabilize because the multiphonon effects in this limit are neglected (see figure 7).

### DEBPs on the RFS for a QD driven by two fields within the full polaron framework

The polaron rate includes the multiphonon effects and is valid in both low and high temperatures. This takes into account the renormalization of the Rabi frequencies  $\Omega$  and  $G$ , and the total damping rate is  $\Gamma_T = \Gamma + \Gamma_p$ .

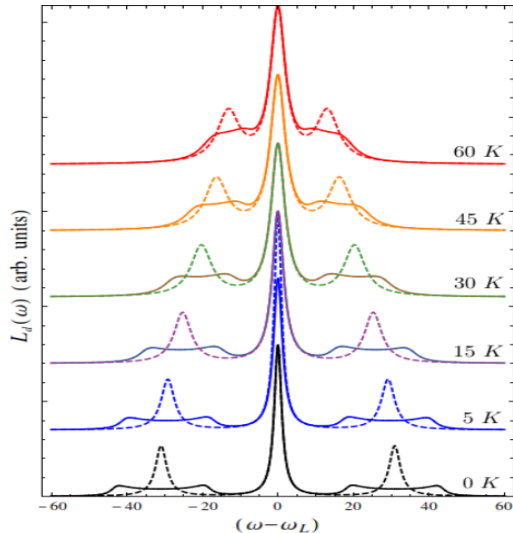


FIG. 8. DEBPs on the RFS of a QD driven by one (dashed lines) and two (solid lines) electromagnetic fields within the full polaron framework.

Figure 8 shows the DEBPs on the RFS of a doubly dressed QD with increasing temperature within the full polaron rate. The polaron rate is similar to the single-phonon polaron rate, but its effects are more pronounced at high temperatures  $T > 40$  K and the peak intensities decrease noticeably with the increasing temperature.

A clear comparison between the three damping rate models is shown in figure 9. There, the difference between the results obtained with either the single phonon or the full polaron approaches at high temperatures (60 K), can be appreciated.

### SUMMARY AND CONCLUSIONS

We have studied theoretically and computationally dissipation effects by phonons on the resonance fluorescence of an artificial atom (or quantum dot) driven by one and two electromagnetic fields, under the assumption that these effects can be captured entirely by renormalization of the Rabi frequencies and inclusion of pure dephasing rates [10, 19].

The model for describing a two-level system driven simultaneously by two electromagnetic fields was revised [7], and expanded with the insertion of phonon effects on the resonance fluorescence spectrum. This spectrum was simulated for realistic parameters of an artificial

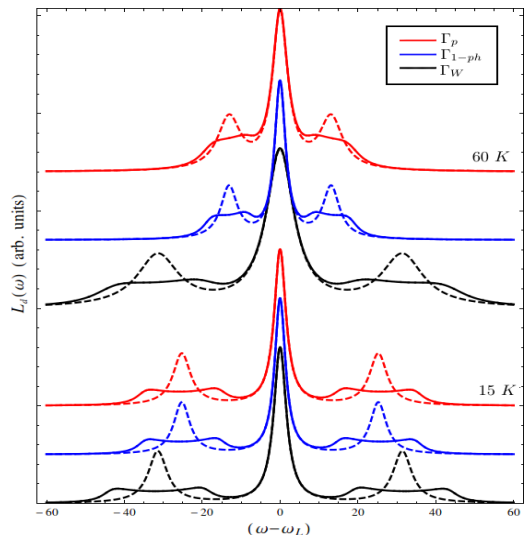


FIG. 9. Comparison of the DEBPs according to the weak-coupling (black line), single-phonon polaron (blue line) and full polaron (red line) approaches, on the RFS of a QD driven by one (dashed lines) and two (solid lines) electromagnetic fields at 15 K and 60 K.

atom [10], and with different models for the coupling of the confined exciton with a longitudinal acoustic phonon environment. Resonance fluorescence spectra calculated within the weak coupling, single-phonon polaron and full polaron approaches, were compared and analyzed in a temperature range between (0 – 60 K).

Our result for dissipation effects in doubly driven QD were obtained by adapting and implementing methods recently proposed and successfully verified in singly driven artificial atoms [5, 9, 10, 20–25], so that they are expected to provide an accurate insight on the temperature dependence of this promising and innovative optical set up.

The calculated resonance fluorescence spectra represent a tool to determine the temperature window in which the proposed scheme would become useful for optoelectronic applications (reliable and robust operation). On one hand, intensity ratio between dark and bright frequencies should be significant; and on the other, gaps between ranges of bright frequencies should be noticeably larger than the corresponding central peak width.

The tunable excitation by two electromagnetic fields has potential applications and repercussions in high quality single photon generation [26, 27], selective filtering of optically active frequencies [28], quantum dot based thermometry [29], and from a more fundamental point of view, stimulates research on quantum interference phenomena in solid-state and quantum manifestations in mesoscopic systems [30, 31].

## ACKNOWLEDGEMENTS

The authors acknowledge the Research Division of Universidad Pedagógica y Tecnológica de Colombia for financial support.

---

\* hanz.ramirez@uptc.edu.co

- [1] E. Burstein and C. Weisbuch, *Confined Electrons and Photons: New Physics and Applications*, Nato Science Series B: (Springer US, 2012).
- [2] P. W. Fry, I. E. Itskevich, D. J. Mowbray, M. S. Skolnick, J. J. Finley, J. A. Barker, E. P. O'Reilly, L. R. Wilson, I. A. Larkin, P. A. Maksym, et al., *Physical Review Letters* **84**, 733 (2000).
- [3] P. Machnikowski and L. Jacak, *Physical Review B* **69**, 193302 (2004).
- [4] B. Mollow, *Physical Review* **188** (1969).
- [5] E. B. Flagg, A. Muller, J. W. Robertson, S. Founta, D. G. Deppe, M. Xiao, W. Ma, G. J. Salamo, and C. K. Shih, *Nature Physics* **5**, 2030 (2009).
- [6] A. N. Vamivakas, Y. Zhao, C.-Y. Lu, and M. Atatüre, *Nature Physics* **5**, 198 (2009).
- [7] H. S. Freedhoff and Z. Ficek, *Physical Review A* **55**, 1234 (1997).
- [8] H. Y. Ramírez, *RSC Advances* **3**, 24991 (2013).
- [9] Y. He, Y.-M. He, J. Liu, Y.-J. Wei, H. Y. Ramírez, M. Atatüre, C. Schneider, M. Kamp, S. Höfling, C.-Y. Lu, et al., *Physical Review Letters* **114** (2015).
- [10] Y.-J. Wei, Y. He, Y.-M. He, C.-Y. Lu, J.-W. Pan, C. Schneider, M. Kamp, S. Höfling, D. P. S. McCutcheon, and A. Nazir, *Physical Review Letters* **113**, 097401 (2014).
- [11] D. P. S. McCutcheon and A. Nazir, *Physical Review Letters* **110**, 217401 (2013).
- [12] H. Freedhoff and T. Quang, *Journal of the Optical Society of America B* **10**, 1337 (1993).
- [13] C. Cohen-Tannoudji, J. Dupont-Roc, and G. Grynberg, *Atom-Photon Interactions: Basic Processes and Applications* (Wiley-Interscience, 1998).
- [14] C. Cohen-Tannoudji, B. Diu, and F. Laloë, *Quantum Mechanics* (Wiley-Interscience, 1977).
- [15] A. Ramsay, A. V. Gopal, E. Gauger, A. Nazir, B. W. Lovett, A. Fox, and M. Skolnick, *Physical Review Letters* **104**, 017402 (2010).
- [16] B. Krummheuer, V. M. Axt, and T. Kuhn, *Physical Review B* **65**, 195313 (2002).
- [17] G. Mahan, *Many-Particle Physics* (Plenum, New York, 1990).
- [18] A. Würger, *Physical Review B* **57**, 347 (1998).
- [19] D. P. McCutcheon and A. Nazir, *New Journal of Physics* **12**, 113042 (2010).
- [20] C. Roy and S. Hughes, *Physical Review B* **85**, 115309 (2012).
- [21] A. Muller, E. B. Flagg, P. Bianucci, X. Wang, D. G. Deppe, W. Ma, J. Zhang, G. Salamo, M. Xiao, and C.-K. Shih, *Physical Review Letters* **99**, 187402 (2007).
- [22] S. Ates, S. Ulrich, S. Reitzenstein, A. Löffler, A. Forchel, and P. Michler, *Physical Review Letters* **103**, 167402 (2009).
- [23] C. Roy and S. Hughes, *Physical Review Letters* **106**, 247403 (2011).
- [24] A. Moelbjerg, P. Kaer, M. Lorke, and J. Mrk, *Physical Review Letters* **108**, 017401 (2012).
- [25] S. Weiler, A. Ulhaq, S. Ulrich, D. Richter, M. Jetter, P. Michler, C. Roy, and S. Hughes, *Physical Review B* **86**, 241304 (2012).
- [26] J. Reithmaier, G. Sek, A. Löffler, C. Hofmann, S. Kuhn, S. Reitzenstein, L. Keldysh, V. Kulakovskii, T. Reinecke, and A. Forchel, *Nature* **432**, 197 (2004).
- [27] K. Hennessy, A. Badolato, M. Winger, D. Gerace, M. Atatüre, S. Gulde, S. Fält, E. L. Hu, and A. Imamoglu, *Nature* **445**, 896 (2007).
- [28] K. J. Vahala, *Nature* **424**, 839 (2003).
- [29] D. M. Toyli, F. Charles, D. J. Christle, V. V. Dobrovitski, and D. D. Awschalom, *Proceedings of the National Academy of Sciences* **110**, 8417 (2013).
- [30] S. Ates, I. Agha, A. Gulinatti, I. Rech, M. T. Rakher, A. Badolato, and K. Srinivasan, *Physical Review Letters* **109**, 147405 (2012).
- [31] T. Brandes, *Physics Reports* **408**, 315 (2005).